Nanoscale

PAPER

View Article Online
View Journal | View Issue

Cite this: *Nanoscale*, 2024, **16**, 1282

H_2O_2-stimulated Janus-shaped self-propelled nanomotors as an active treatment for acute renal injury†

Jun Xu, *‡[a] Yali Zhong,‡[b] Weixin Wang,‡[c] Rui Gao,‡[c] Yini Wang,‡[c] Fei Tong, ‡[c,d,e] Jiahui Sun,[c] Miaofang Hong,[c] Lingyan Qiao,[c] Weiwei Qiao,[c] Qibing Mei[e,f] and Jianming Wu [e,f]

Received 23rd September 2023,
Accepted 7th November 2023

DOI: 10.1039/d3nr04808j

rsc.li/nanoscale

As emerging nanosystems, nanomotors have been applied in the active treatment of many diseases. In this paper, Pt@chitosan-loaded melatonin asymmetrical nanomaterials embedded with L-serine (S, kidney injury molecule 1-targeting agent) were constructed to alleviate acute kidney injury (AKI). The Janus nanocarriers arrived at the renal injury site *via* the bloodstream and exhibited high permeability. Because of melatonin distribution in the kidneys combined with H_2O_2-stimulated O_2 release, the administration of the Janus nanosystem resulted in active treatment through the motion of nanomotors by asymmetrical O_2 release.

Introduction

Acute kidney injury (AKI) is a clinical syndrome induced by a variety of factors, mainly decreased renal function, tubular and glomerular damage, and reduced or absent urine.[1] It has become a major public health problem, affecting millions of patients worldwide and leading to decreased survival rates.[2] Although many experts and scholars have studied AKI in the past few decades, the complex pathophysiology of AKI is not fully understood, and suitable therapy to prevent or treat AKI has not been determined.[3] However, nanotechnology-based drug delivery targeting renal tubules has provided a new strategy for AKI therapy.[4–10]

Although many nanomedicines are now used to treat AKI,[4–10] these nanodrugs are delivered by passive diffusion, and their targeting and selectivity are very poor and they are unable to achieve true active treatment.[11,12] Micro/nanomotors have undergone rapid development in recent years and can now be readily propelled in different environments and display better functions than their static counterparts *in vitro*/

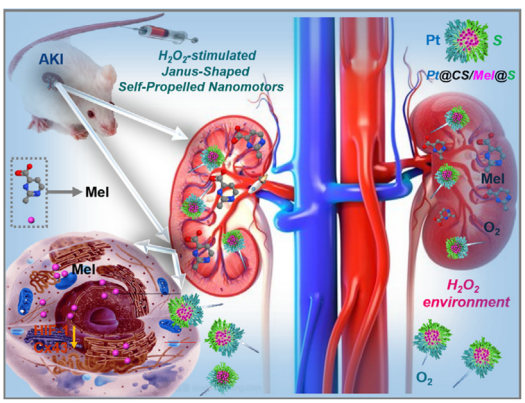

Scheme 1 Schematic illustration of the synthesis and therapeutic process of PCMS nanomotors. 'Mel' was first loaded into CS, and 'S' was then attached on one side, followed by surface attachment of Pt on the opposite side. An H_2O_2-rich environment resulted in O_2/Mel release, and the diffusion of O_2 accelerated the motion of the nanomotors and further promoted AKI treatment.

[a]*Department of Emergency, First Affiliated Hospital of Jiaxing University, Jiaxing, Zhejiang Province, China. E-mail: jiaxingxujun@163.com*
[b]*Southwest University of Science and Technology, Mianyang, 621000, China. E-mail: 804237965@qq.com*
[c]*College of Pharmacy, Binzhou Medical University, Yantai, 264003, PR China. E-mail: BZwangyini@163.com, 3155573681@qq.com, tongxuchang@163.com, 15065257158@163.com, 1223385134@qq.com, 2162567696@qq.com, joann_1029@163.com, qwwi5@126.com*
[d]*School of Basic Medical Sciences, Zhejiang University Medicine, Hangzhou, 310000, PR China*
[e]*Education Ministry Key Laboratory of Medical Electrophysiology, Sichuan Key Medical Laboratory of New Drug Discovery and Druggability Evaluation, Luzhou, China*
[f]*Key Laboratory of Activity Screening and Druggability Evaluation for Chinese Materia Medica, School of Pharmacy, Southwest Medical University, Luzhou, 646000, China. E-mail: qbmei53@hotmail.com, jianmingwu@swmu.edu.cn*

†Electronic supplementary information (ESI) available. See DOI: https://doi.org/10.1039/d3nr04808j

‡These authors contributed equally to this work.

in vivo.[11,12] Based on immense research progress on the use of micro/nanomotors,[11,12] we developed H_2O_2-stimulated Janus-shaped self-propelled nanomotors that could improve the delivery of melatonin for the treatment of AKI.

The H_2O_2-activated nanomotors were synthesized by modifying the surface of melatonin (Mel)-loaded chitosan (CS) with the kidney tubule-targeting moiety L-serine ('S') on one side while further attaching Pt to the opposite side (the nanomotors are hereafter referred to as Pt@CS/Mel@S (PCMS) nanomotors, Scheme 1). The nanomotors accumulate in the kidney tubule due to the high affinity of "S" for Kim-1 (kidney injury molecule-1), leading to the fast release of Mel from PCMS into the high-H_2O_2 environment. Due to the asymmetrical nature of the nanomotors, the asymmetrical release of O_2 propels the nanomotors. Moreover, the released O_2/Mel could improve the hypoxic environment, attenuate ROS transmission between adjacent cells and oxidative stress suppression in AKI by down-regulating the Cx43 expression. To the best of our knowledge,

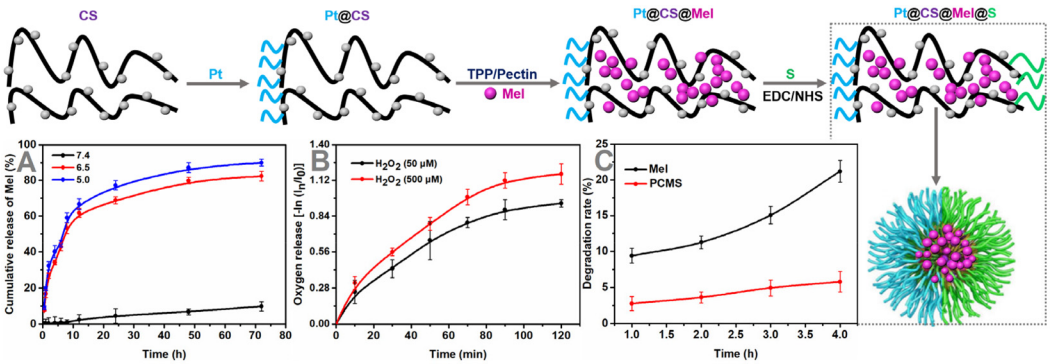

Fig. 1 *In vitro* release. (A) Cumulative release of Mel from PCMS at different pH values (7.4/6.5/5.0). (B) O_2 release from PCMS in different H_2O_2 concentrations (50 and 500 μM). (C) Degradation rate of PCMS under visible light (PCMS, Pt@CS/Mel@S; Mel, melatonin; CS, chitosan; S, L-serine); n = 5.

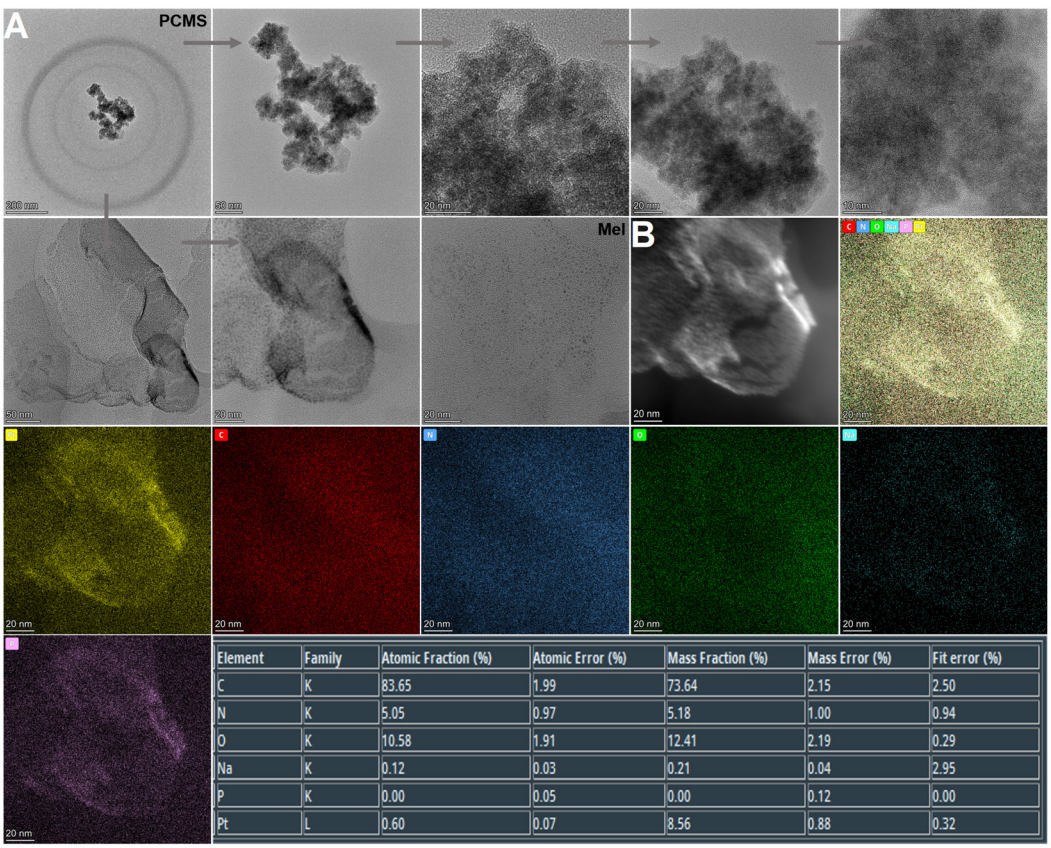

Element	Family	Atomic Fraction (%)	Atomic Error (%)	Mass Fraction (%)	Mass Error (%)	Fit error (%)
C	K	83.65	1.99	73.64	2.15	2.50
N	K	5.05	0.97	5.18	1.00	0.94
O	K	10.58	1.91	12.41	2.19	0.29
Na	K	0.12	0.03	0.21	0.04	2.95
P	K	0.00	0.05	0.00	0.12	0.00
Pt	L	0.60	0.07	8.56	0.88	0.32

Fig. 2 TEM analysis. (A) TEM of PCMS. (B) EDS mapping of PCMS (PCMS, Pt@CS/Mel@S; Mel, melatonin; CS, chitosan; S, L-serine).

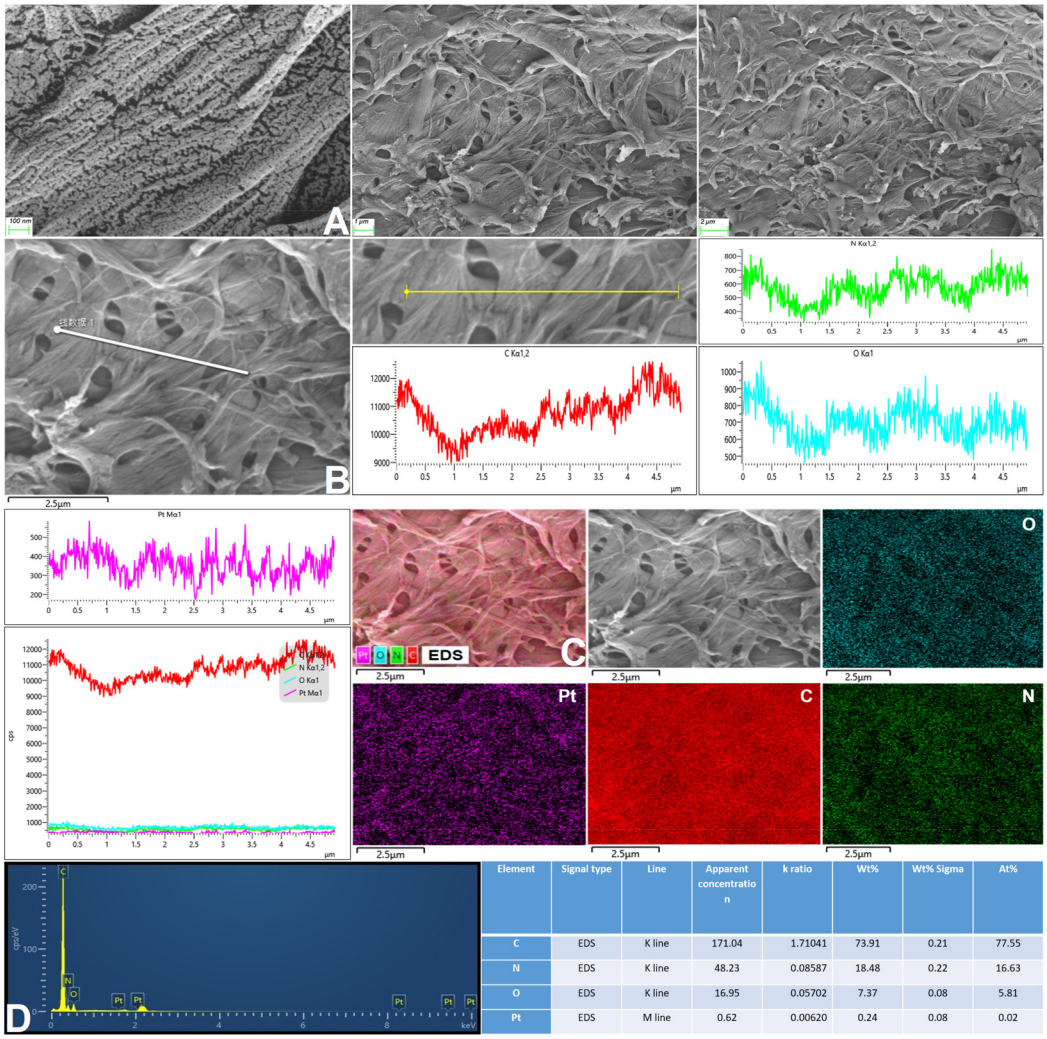

Fig. 3 SEM analysis. (A) SEM of PCMS (100 nm, 1 μm and 2 μm). (B) Total number of distribution graphs. (C and D) EDS mapping and linear total spectrogram of PCMS (PCMS, Pt@CS/Mel@S; Mel, melatonin; CS, chitosan; S, L-serine).

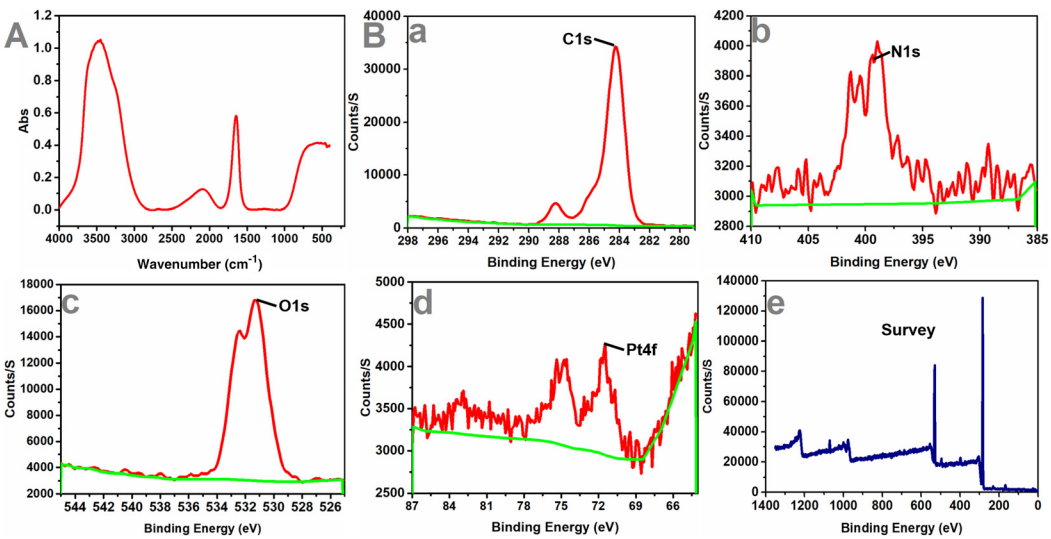

Fig. 4 *In vitro* characterization. (A) FT-IR analysis of PCMS. (B) XPS analysis of PCMS (a, C 1s; b, N 1s; c, O 1s; d, Pt 4f; and e, survey spectra) (PCMS, Pt@CS/Mel@S; Mel, melatonin; CS, chitosan; S, L-serine).

the H_2O_2-activated nanomotors, which have motor function and can asymmetrically release and actively deliver O_2/Mel, significantly act in the treatment of AKI *in vivo*. Our findings/results might not only enlarge the biomedical applications of nanomotors but also supply novel theoretical evidence and/or foundations for the research of treatments for kidney damnification.

Results

Characterization of Pt@CS/Mel@S (PCMS) nanomotors

As shown in Fig. 1, Mel was incubated with chitosan (CS) (synthesized as described in a previous document to achieve successful drug loading).[13] After dialysis to dispel free melatonin (Mel), the ratio of drugs that was successfully loaded on Pt@CS was ~11.78%, which was calculated by an ultraviolet absorption spectrum. The kidney tubule targeting moiety L-serine ('S') was attached to one side of Pt@CS/Mel, with a grafting ratio of ~9.04%, which was calculated by the ultraviolet absorption spectrum (Fig. S1 and 2, ESI†).

Subsequently, the amounts of Mel released from PCMS nanomotors at pH 7.4/6.5/5.0 were assessed, and the results are shown in Fig. 1A, revealing long-term pH-triggered Mel release from the PCMS nanomotors. This might be due to the amino protonation of CS in PCMS under acidic conditions, disrupting the intermolecular hydrogen bonding of CS and damaging the secondary structure, resulting in increased Mel release.[14,15] In addition, O_2 release from PCMS nanomotors under H_2O_2-rich conditions was observed, and the results are shown in Fig. 1B, confirming the fabrication of H_2O_2-stimulated Janus-shaped O_2-propelled nanomotors. The degradation rate of Mel in an aqueous solution of Mel and PCMS under light irradiation is shown in Fig. 1C, and the results indicate

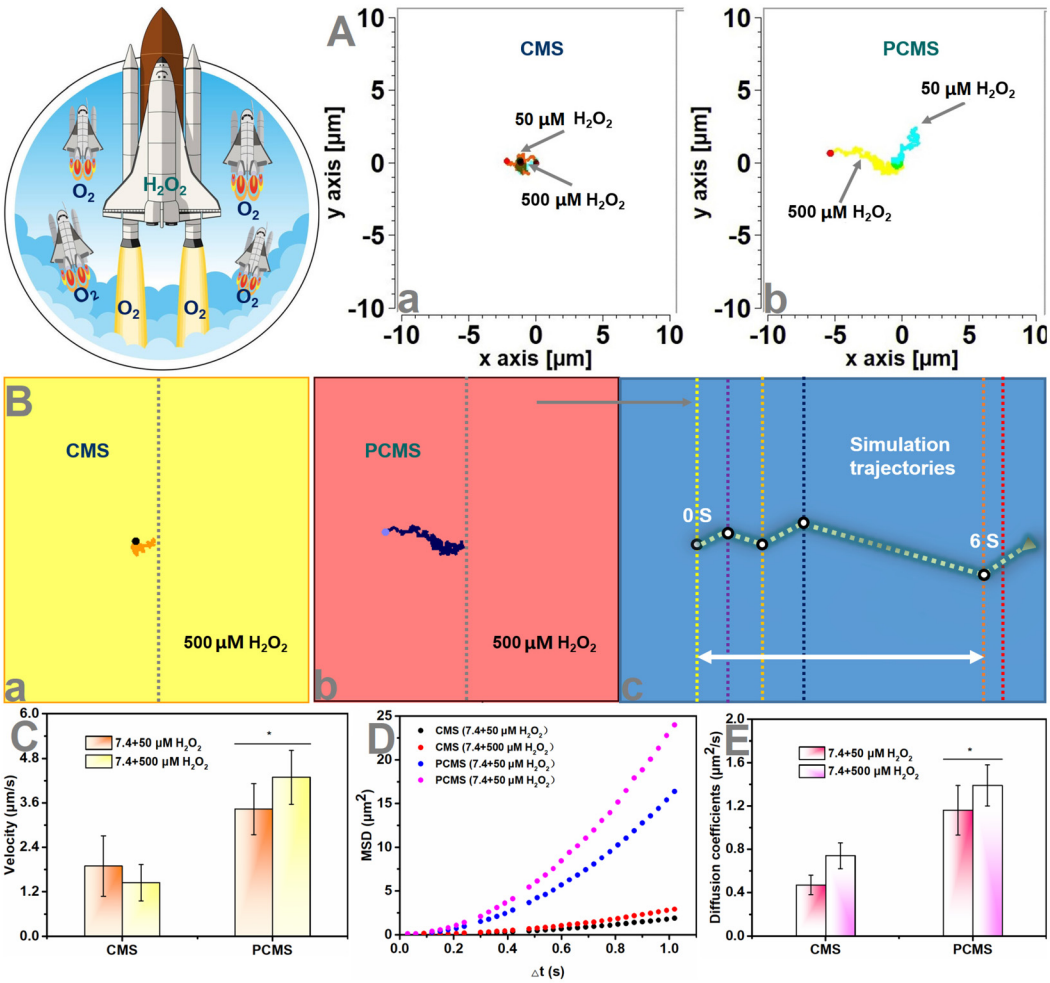

Fig. 5 Motion of nanomotors. (A) Motion trajectories (10 s) of PCMS nanomotors at different H_2O_2 concentrations (a, CMS; b, PCMS). (B) Time-lapse images of PCMS nanomotors at different H_2O_2 concentrations (50 and 500 μM H_2O_2) (a, CMS; b, PCMS; c, simulation trajectories). (C) The velocity of PCMS nanomotors at different H_2O_2 concentrations (50 and 500 μM H_2O_2). (D) MSD of PCMS nanomotors at different H_2O_2 concentrations (50 and 500 μM H_2O_2). The directional motion was fitted to the equation $(4D)\Delta t + (V^2)(\Delta t^2)$, and the Brownian motion was fitted to the equation $(4D)\Delta t$. (E) The diffusion coefficients of PCMS nanomotors at different H_2O_2 concentrations (50 and 500 μM H_2O_2) (CMS, CS/Mel@S; PCMS, Pt@CS/Mel@S; Mel, melatonin; CS, chitosan; S, L-serine); n = 20.

that PCMS could effectively reduce Mel degradation and prolong its holding time. This might be due to the photodegradation of Mel, which could be caused by the formation of peroxide intermediates in the indole ring under conditions of light and oxygen, whereupon it rapidly becomes a stable product, N1-acetyl-N2-formyl-5-methoxycaninurine. The decrease in photodegradation of PCMS could be related to the reduction of Mel's direct contact with light and oxygen due to the chitosan shell. This feature utilized PCMS to enhance the pharmacological effects of Mel under unrestricted dark conditions.

After successful synthesis, the samples were characterized by TEM, EDS mapping and SEM (Fig. 2A, B and 3), and it was determined from the TEM images that the average size of the structure was 139.3 nm.

Next, the particle size change of the samples was observed. The results are shown in Fig. S3, ESI† and the average particle size was 176.04 nm. In addition, FT-IR spectroscopy and XPS were performed to study the chemical composition of the nanomotors (Fig. 4). The peak values of each element in the graphs indicated that the PCMS nanomotors were successfully obtained.

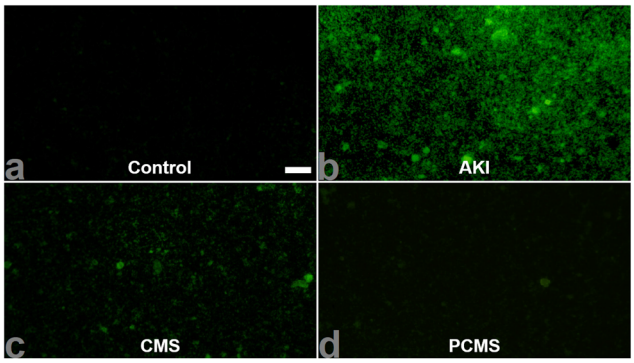

Fig. 6 ROS observation *in vitro*. ROS production after different treatments by inverted immunofluorescence microscopy (a, control; b, AKI; c, CMS; d, PCMS) (CMS, CS/Mel@S; PCMS, Pt@CS/Mel@S; Mel, melatonin; CS, chitosan; S, L-serine). Scale bar: 50 μm.

Autonomous motion of nanomotors

After exploring the successful *in vitro* synergistic process (results contained in Fig. 2–4 and Fig. S1–3, ESI†) of PCMS, we next measured the H_2O_2 response-induced motion of PCMS in PBS with different H_2O_2 concentrations. An inverted fluorescence microscope equipped with a charge-coupled device (CCD) camera was used to record the movement of PCMS in real time for 10 s to create a video with 10 frames per second. In an H_2O_2-rich environment, the motion of PCMS was increased compared to that of non-H_2O_2 conditions (Fig. 5A, B, Fig. S4, ESI and Videos S1–3†). The mean square displace-

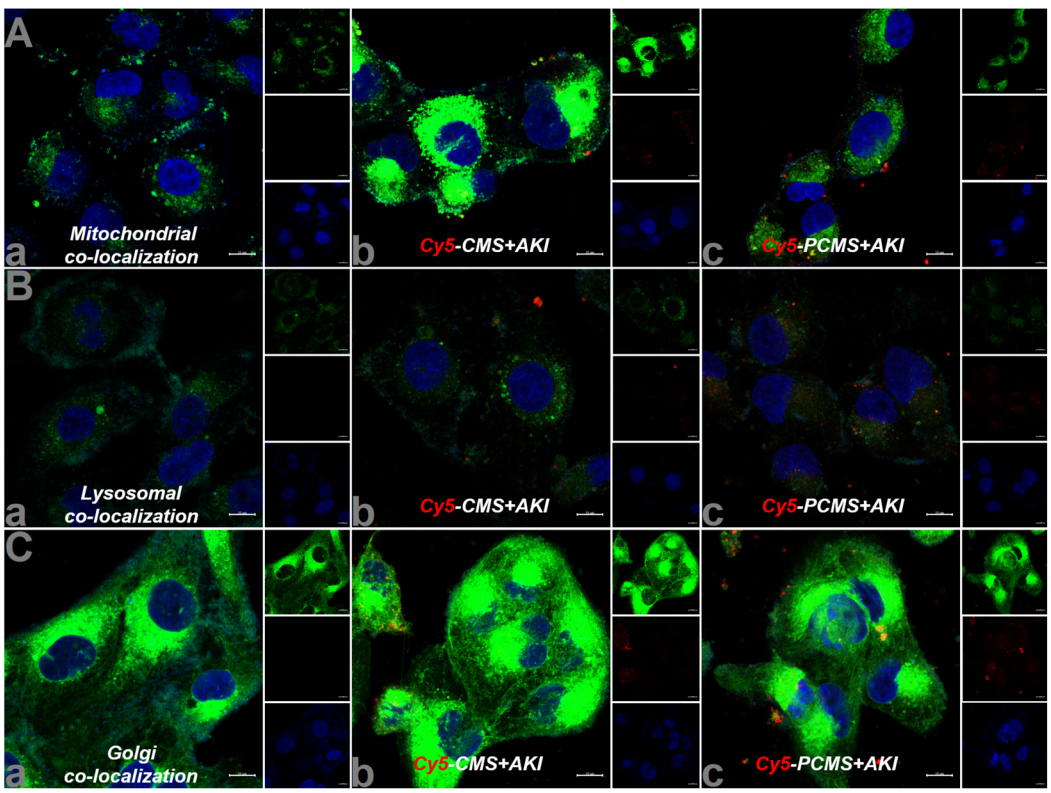

Fig. 7 Colocalization by confocal microscopy. (A) Colocalization of Cy5-PCMS in mitochondria (green light, MitoTracker® Green FM). (B) Colocalization of Cy5-PCMS in lysosomes (green light, Lyso-Tracker Green). (C) Colocalization of Cy5-PCMS in the Golgi (green light, Golgi-Tracker Green). (a, control; b, Cy5-CMS + AKI; c, Cy5-PCMS + AKI.) (CMS, CS/Mel@S; PCMS, Pt@CS/Mel@S). Scale bar: 100 μm.

ment (MSD) was further obtained by simultaneously recording the x,y coordinates of multiple particles (20 particles) based on nanoparticle tracking analysis. Fitting the MSD curves allowed the average velocity of PCMS to be calculated by using the self-diffusion model.[16–24] Subsequently, the obtained MSD (Fig. 5D and Fig. S4, ESI†) and velocity values (Fig. 5C and Fig. S4, ESI†) of the H_2O_2-activated nanomotors indicated directional and autonomous movement compared to that of non-H_2O_2 conditions. The PCMS motors moved from the opening to the bottom in PBS (H_2O_2, 500 μM) with a velocity of up to 4.29 μm s^{-1}. Both the MSD and velocities were enhanced, possibly because more O_2 was released from PCMS due to the H_2O_2 environment. However, Brownian motion was observed, and the MSD curve had a representative shape (linear) and size, indicating Brownian motion in the absence of an H_2O_2-rich environment (Fig. 5D and Fig. S4, ESI†). The representative diffusion coefficient and tracking trajectories of PCMS with and without H_2O_2 are further presented in Fig. 5E, A and Fig. S4, ESI,† respectively. The diffusion coefficient of CMS in PBS (pH 7.4 + H_2O_2, 500 μM) was 0.74 μm^2 s^{-1}, and that of PCMS increased to 1.39 μm^2 s^{-1} in PBS (pH 7.4 + H_2O_2, 500 μM), indicating active self-propulsion.

Cell evaluation

After the completion of the *in vitro* nanomotor motion evaluation, we subsequently observed the effect of nanomotors on human renal tubular epithelial (HKC) cell viability. The results are shown in Fig. S5, ESI,† revealing that the HKC cell viability still reached above 80% with administration of PCMS (200 μg mL^{-1}), indicating that PCMS had no obvious toxic effect. Next, through the literature, *in vitro* acute kidney injury (AKI) was reproduced,[11,12] and H_2O_2 and ROS levels in AKI *in vitro* were significantly increased when compared to the control group. However, PCMS treatment can obviously reduce the contents of H_2O_2 and ROS, as shown in Fig. 6 and Fig. S6 and 7, ESI.† These results show that PCMS could significantly reduce the oxidative stress injury in AKI *in vitro*.

In addition, colocalization of PCMS in AKI *in vitro* was inspected, and the results, as shown in Fig. 7, imply that PCMS could effectively enter mitochondria, lysosomes and the

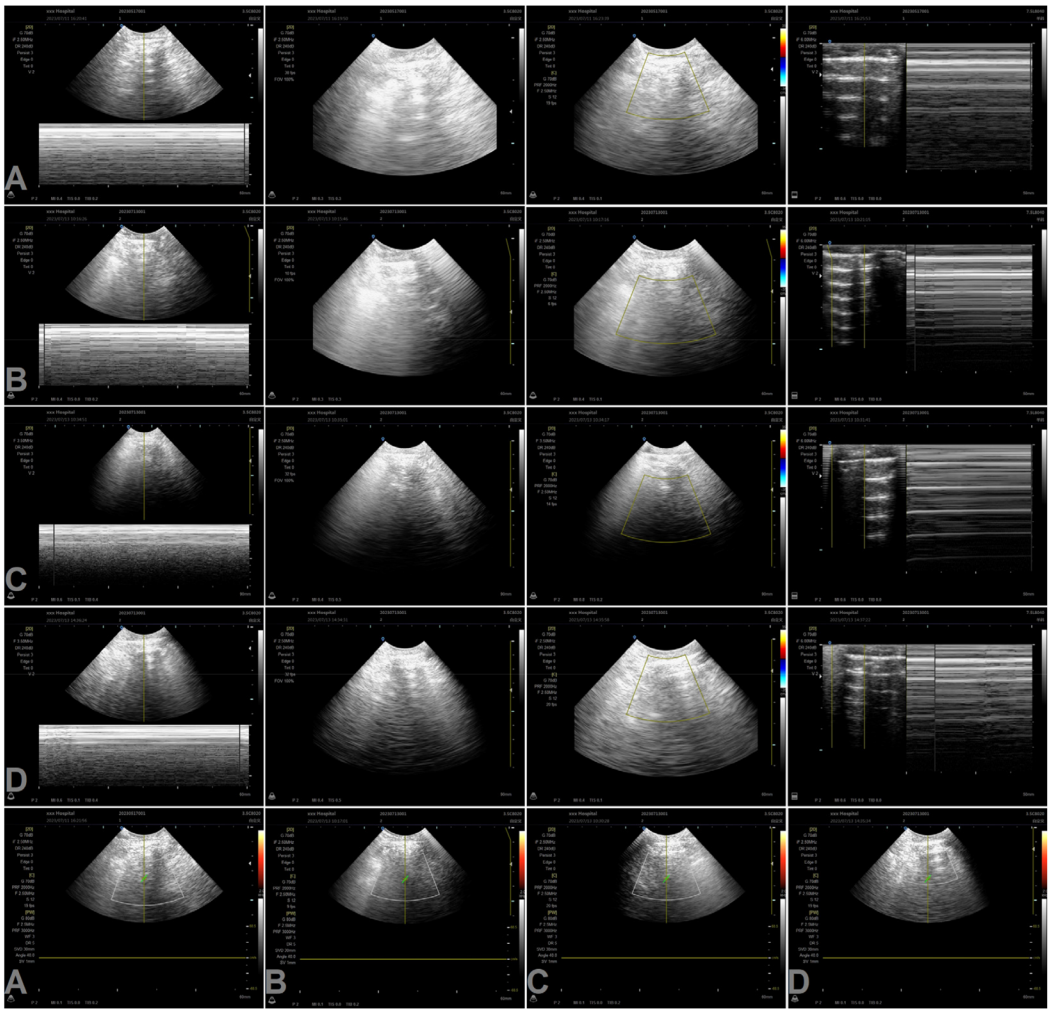

Fig. 8 *In vivo* renal blood flow and renal tissue change by B-scan ultrasonography. (A) Control. (B) AKI. (C) PCM. (D) PCMS (PCMS, Pt@CS/Mel@S; PCM, Pt@CS/Mel).

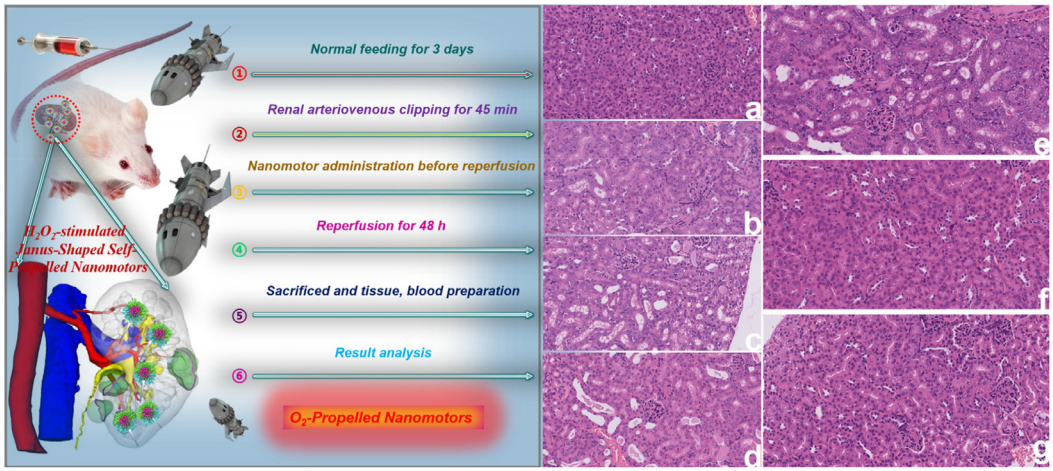

Fig. 9 *In vivo* HE staining. HE staining of different tissues after different treatments (a, control; b, AKI; c, Mel; d, CM; e, PCM; f, CMS; g, PCMS) (CM, CS/Mel; PCM, Pt@CS/Mel; CMS, CS/Mel@S; PCMS, Pt@CS/Mel@S; Mel, melatonin; CS, chitosan; S, L-serine). Scale bar: 50 μm.

Golgi in AKI *in vitro* to release drugs, ultimately alleviating AKI *in vitro.*

In vivo dispersion and renal blood flow changes

After evaluating cell effects *in vitro*, we observed the dispersion of nanomotors *in vivo*. As shown in Videos S4–6 and Fig. S8 and 9, ESI,† these observations indicate that PCMS accumulates and their concentration increases in the kidneys after entering the body for 4 h, and remain enriched in the kidneys after 48 h. Subsequently, the renal blood flow and renal tissue were measured following PCMS treatment, as shown in Fig. 8. The results showed that PCMS treatment could have anti-AKI effects and improve renal blood flow.

In vivo pharmacodynamics

Next, we assessed the renal function effect of PCMS. As shown in Fig. S10, ESI,† the blood urea nitrogen (BUN) and blood creatinine (Scr) levels significantly increased in AKI but PCMS treatment could dramatically downregulate the contents of BUN and Scr, with these results indicating that PCMS obviously ameliorated renal function compared to that seen in the control group. In addition, PCMS also significantly decreased oxygen free radical damage, as shown in Fig. S11 and 12, ESI.† In AKI, the superoxide dismutase (SOD) level is less than that of the control group, while the contents of malondialdehyde (MDA), hydrogen peroxide (H_2O_2), and reactive oxygen species (ROS) are more than those in the control group. However, administration of PCMS obviously enhanced the SOD and reduced the MDA, H_2O_2, and ROS levels. Then, we further observed the HE and TUNEL changes after PCMS administration, as shown in Fig. 9 and 10. Pathological damage and cell apoptosis in renal tissue evidently increases in AKI, but PCMS treatment can clearly improve the injury and these results indicate that PCMS has an obvious anti-AKI effect.

The results of immunohistochemical and immunofluorescence analyses are shown in Fig. S13–15, ESI.† The expressions of kidney injury molecule 1 (Kim-1), connexin 43 (Cx43) and hypoxia inducible factor-1α (HIF-1α) are significantly upregulated in AKI but PCMS treatment could obviously downregulate these expressions. These results show that PCMS could significantly reduce the expressions of Kim-1, Cx43 and HIF-1α to

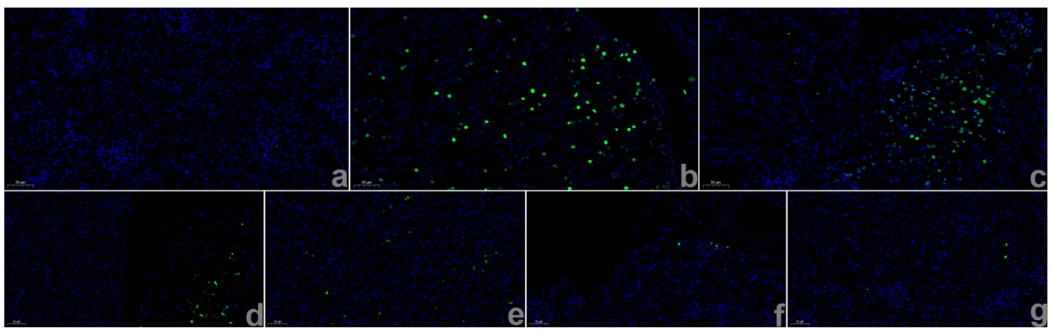

Fig. 10 *In vivo* TUNEL staining. TUNEL staining of different tissues after different treatments (a, control; b, AKI; c, Mel; d, CM; e, PCM; f, CMS; g, PCMS) (CM, CS/Mel; PCM, Pt@CS/Mel; CMS, CS/Mel@S; PCMS, Pt@CS/Mel@S; Mel, melatonin; CS, chitosan; S, L-serine). Scale bar: 50 μm.

attenuate ROS transmission between adjacent cells, inhibit oxidative stress, and ameliorate the hypoxic environment, thereby alleviating AKI.

Conclusion

We synthetized O_2-driven nanomotors based on a biochemical reaction *in vitro* and *in vivo*. O_2 not only serves as the power source of these nanomotors to promote drug release deep into renal sites of AKI, but also acts as a therapeutic drug itself. The synergistic function of O_2 and Mel could ameliorate AKI, thus inhibiting apoptosis and downregulating Cx43 expression. Moreover, downregulating Cx43 expression showed that O_2-driven nanomotors could inhibit obvious gap connections and regulate ROS levels to reduce AKI. Ultimately, *in vitro*/*in vivo* experiments confirmed the good therapeutic effect of the O_2-driven nanomotors.

Data availability

All data needed to assess the results in this article are presented in the article and/or the ESI.† Additional data related to the article may be requested from the authors.

Author contributions

J. X. conceived and designed the experiments. J. X. performed the experiments, analysed the data and drafted the manuscript. All authors discussed the results and contributed to the final form of the manuscript.

Conflicts of interest

The authors declare no competing interests.

Acknowledgements

We acknowledge support from the General scientific research project of Zhejiang Education Department (Y202249584) and Jiaxing Key Discipline of Medicine-Emergency Medicine (2023-ZC-004).

References

1 J. Sun, J. Zhang, J. Tian, *et al.*, Mitochondria in sepsis-induced AKI, *J. Am. Soc. Nephrol.*, 2019, **30**, 1151–1161.
2 K. Singbartl and J. A. Kellum, AKI in the ICU: definition, epidemiology, risk stratification, and outcomes, *Kidney Int.*, 2012, **81**, 819–825.
3 E. Kwiatkowska, L. Domański, V. Dziedziejko, *et al.*, The mechanism of drug nephrotoxicity and the methods for preventing kidney damage, *Int. J. Mol. Sci.*, 2021, **22**, 6109.
4 H. Yu, T. Lin, W. Chen, *et al.*, Size and temporal-dependent efficacy of oltipraz-loaded PLGA nanoparticles for treatment of acute kidney injury and fibrosis, *Biomaterials*, 2019, **219**, 119368.
5 N. Kamaly, J. C. He, D. A. Ausiello, *et al.*, Nanomedicines for renal disease: current status and future applications, *Nat. Rev. Nephrol.*, 2016, **12**, 738–753.
6 R. M. Williams, E. A. Jaimes and D. A. Heller, Nanomedicines for kidney diseases, *Kidney Int.*, 2016, **90**, 740–745.
7 G. T. Tietjen, S. A. Hosgood, J. DiRito, *et al.*, Nanoparticle targeting to the endothelium during normothermic machine perfusion of human kidneys, *Sci. Transl. Med.*, 2017, **9**, eaam6764.
8 J. Wang, J. J. Masehi-Lano and E. J. Chung, Peptide and antibody ligands for renal targeting: nanomedicine strategies for kidney disease, *Biomater. Sci.*, 2017, **5**, 1450–1459.
9 R. M. Williams, J. Shah, B. D. Ng, *et al.*, Mesoscale nanoparticles selectively target the renal proximal tubule epithelium, *Nano Lett.*, 2015, **15**, 2358–2364.
10 S. Gao, S. Hein, F. Dagnaes-Hansen, *et al.*, Megalin-mediated specific uptake of chitosan/siRNA nanoparticles in mouse kidney proximal tubule epithelial cells enables AQP1 gene silencing, *Theranostics*, 2014, **4**, 1039–1051.
11 F. Tong, J. Liu, L. Luo, *et al.*, pH/ROS-responsive propelled nanomotors for the active treatment of renal injury, *Nanoscale*, 2023, **15**, 6745–6758.
12 F. Tong, J. Liu, Y. Zhong, *et al.*, Carbon monoxide-propelled nanomotors as an active treatment for renal injury, *Appl. Mater. Today*, 2023, **32**, 101823.
13 B. Zhou, X. Yu, M. Zhang, *et al.*, Melatonin chitosan microparticles decrease degradation and increase drought resistance properties of melatonin, *J. Plant Nutr. Fert.*, 2022, **28**, 1308–1317. (China).
14 A. Geraili, *et al.*, Design and fabrication of drug-delivery systems toward adjustable release profiles for personalized treatment, *VIEW*, 2021, **2**, 20200126.
15 Y. Yang, *et al.*, Smart materials for drug delivery and cancer therapy, *VIEW*, 2021, **2**, 20200042.
16 M. Wan, *et al.*, Zwitterion-based hydrogen sulfide nanomotors induce multiple acidosis in tumor cells by destroying tumor metabolic symbiosis, *Angew. Chem., Int. Ed.*, 2021, **60**, 16139–16148.
17 H. Zhang, Z. Li, C. Gao, *et al.*, Dual-responsive biohybrid neutrobots for active target delivery, *Sci. Robot.*, 2021, **6**, eaaz9519.
18 C. Gao, Y. Wang, Z. Ye, *et al.*, Biomedical Micro-/Nanomotors: From Overcoming Biological Barriers to In Vivo Imaging, *Adv. Mater.*, 2021, **33**, e2000512.
19 H. Li, Y. Li, J. Liu, *et al.*, Asymmetric colloidal motors: from dissymmetric nanoarchitectural fabrication to efficient propulsion strategy, *Nanoscale*, 2022, **14**, 7444–7459.
20 C. Zhou, C. Gao, Y. Wu, *et al.*, Torque-driven orientation motion of chemotactic colloidal motors, *Angew. Chem., Int. Ed.*, 2022, **61**, e202116013.

21 X. Lin, Z. Wu, Y. Wu, *et al.*, Self-propelled micro-/nanomotors based on controlled assembled architectures, *Adv. Mater.*, 2016, **28**, 1060–1072.
22 Y. Ye, F. Tong, S. Wang, *et al.*, Apoptotic tumor DNA activated nanomotor chemotaxis, *Nano Lett.*, 2021, **21**, 8086–8094.
23 L. Liu, J. Wu, B. Chen, *et al.*, Magnetically actuated biohybrid microswimmers for precise photothermal muscle contraction, *ACS Nano*, 2022, **16**, 6515–6526.
24 Y. Feng, C. Gao, D. Xie, *et al.* Directed neural stem cells differentiation via signal communication with Ni-Zn micromotors, *Adv. Mater.*, 2023, e2301736.